ADVANCES IN ATMOSPHERIC SCIENCES, VOL. 34, APIRL 2017, 545–558

• **Original Paper** •

A Ka-band Solid-state Transmitter Cloud Radar and Data Merging Algorithm for Its Measurements

Liping LIU*[1], Jiafeng ZHENG[2], and Jingya WU[1]

[1] *State Key Laboratory of Severe Weather, Chinese Academy of Meteorological Sciences, Beijing* 100086*, China*

[2] *Chengdu University of Information Technology, School of Atmospheric Sciences, Chengdu* 610025*, China*

(Received 24 March 2016; revised 15 August 2016; accepted 13 September 2016)

ABSTRACT

This study concerns a Ka-band solid-state transmitter cloud radar, made in China, which can operate in three different work modes, with different pulse widths, and coherent and incoherent integration numbers, to meet the requirements for cloud remote sensing over the Tibetan Plateau. Specifically, the design of the three operational modes of the radar (i.e., boundary mode M1, cirrus mode M2, and precipitation mode M3) is introduced. Also, a cloud radar data merging algorithm for the three modes is proposed. Using one month's continuous measurements during summertime at Naqu on the Tibetan Plateau, we analyzed the consistency between the cloud radar measurements of the three modes. The number of occurrences of radar detections of hydrometeors and the percentage contributions of the different modes' data to the merged data were estimated. The performance of the merging algorithm was evaluated. The results indicated that the minimum detectable reflectivity for each mode was consistent with theoretical results. Merged data provided measurements with a minimum reflectivity of −35 dBZ at the height of 5 km, and obtained information above the height of 0.2 km. Measurements of radial velocity by the three operational modes agreed very well, and systematic errors in measurements of reflectivity were less than 2 dB. However, large discrepancies existed in the measurements of the linear depolarization ratio taken from the different operational modes. The percentage of radar detections of hydrometeors in mid- and high-level clouds increased by 60% through application of pulse compression techniques. In conclusion, the merged data are appropriate for cloud and precipitation studies over the Tibetan Plateau.

Key words: data merging algorithm, operational mode, Ka-band radar, cloud, Tibetan Plateau, pulse compression technique

Citation: Liu, L. P., J. F. Zheng, and J. Y. Wu, 2017: A Ka-band solid-state transmitter cloud radar and data merging algorithm for its measurements. *Adv. Atmos. Sci.*, **34**(4), 545–558, doi:10.1007/s00376-016-6044-8.

1. Introduction

Due to strong surface heating and relatively dry air, clouds and microphysical processes over the Tibetan Plateau are different to those in low-elevation regions. Convection is common over the Tibetan Plateau, but only lasts a short period and its intensity is weak. Clouds and precipitation over the Tibetan Plateau are important for the transport of water vapor and atmospheric heating. Under favorable conditions, synoptic weather systems over the Tibetan Plateau often move out of the region, causing rainstorms and other disastrous weather events in downwind areas. Cloud radar is an important tool for obtaining vertical structures of clouds and light precipitation. Millimeter-wave cloud radar mainly operates in the Ka-band (with a wavelength of 8 mm) or the W-band (with a wavelength of 3 mm), and the most commonly used transmitters include magnetrons, traveling wave tubes and solid-state transmitters. Ka-band cloud radar is often utilized for long-term monitoring at fixed locations due to its large transmitted power and mature hardware. It can effectively observe various types of clouds, and is able to detect light precipitation. Using radar signal processing techniques, such as spectral analysis, pulse compression, coherent integration and incoherent integration, a variety of operational modes can be used to simultaneously detect clouds at different heights and with different intensity. In the ARM program sponsored by U.S DOE, the Ka-band cloud radar (MMCR) used traveling wave tubes and operated in four different modes that were cycled repetitively. Two of the operational modes used pulse compression techniques to generate high-sensitivity measurements of high clouds, while the other two modes without pulse compression measured low clouds and precipitation. These modes had different spatial resolutions (45 km, 90 km) and maximum detection ranges (10 km, 15 km). The minimum detectable reflectivity at the height of 5 km could be up to −49 dBZ (Moran et al., 1998). After 1997, technical parameters, such as the pulse repetition frequency and the numbers of coherent and incoherent integrations were improved in the MMCR operational

* Corresponding author: Liping LIU
Email: lpliu@camscma.cn

modes. As a result, the minimum detectable reflectivity was reduced to −54 dBZ (Clothiaux et al., 1999). Clothiaux et al. (2000) proposed a radar data processing algorithm that integrated data from various operational modes. Radial velocity aliasing, second-trip echoes, and pulse compression sidelobes were considered in this algorithm, and lidar observations were used to correct the heights of cloud bases. Based on this algorithm, they analyzed the consistency of radar reflectivity measured by different modes. However, they did not analyze the consistency of radial velocity, velocity spectrum width and the linear depolarization ratio ($L_{\rm DR}$). Kollias et al. (2007) further improved the MMCR operational modes by introducing five operational modes, which consisted of a boundary mode, a cirrus mode, a precipitation mode, a general mode, and a polarization mode (Kollias et al., 2007). This multi-mode design improved the detection capability of the cloud radar system. However, for a specific mode, the design of key technical parameters, such as minimum detectable reflectivity, maximum range of detection, unambiguous velocity and radial velocity resolution, had to balance compromises. For example, the pulse compression technique improved the radar sensitivity and detection capability but enlarged the minimum range of useful data. The coherent integration approach increased the radar detection sensitivity but reduced the Nyquist velocity.

In recent years, magnetrons and high-power traveling wave tubes have been adopted for transmitters in the development of millimeter-wave radars in China. The Ka-band cloud radar co-developed at the Chinese Academy of Meteorological Science (CAMS) and the 23rd Institute of China Aerospace Science and Technology Corporation has a peak power of 600 W. The minimum detectable reflectivity at a 10-km range is −25.7 dBZ and −31.3 dBZ, corresponding to pulse widths of 0.3 μs and 1.5 μs. Due to its transmitter duration and lifetime, this cloud radar is only used for periodic measurements at specific time periods. This cloud radar has been deployed in Guangdong, Yunnan and Jilin provinces for cloud and precipitation measurements. Data analysis algorithms have also been developed for cloud radar measurements (Zhong et al., 2011; Liu et al., 2014). In order to obtain continuous and reliable cloud and precipitation measurements, in 2013 CAMS collaborated with the 23rd Institute of China Aerospace Science and Technology Corporation to develop a Ka-band millimeter-wave cloud radar with a solid-state transmitter, which was later utilized during the Third Tibetan Plateau Atmospheric Experiment in 2014 and 2015. This radar adopts pulse compression, as well as coherent and incoherent integration techniques, and operates in three different modes that are cycled repetitively (Liu et al., 2015). Unfortunately, its measurements, from the perspective of the radar's different modes and the consistency among measurements, have yet to be systematically studied and evaluated.

In the present paper, we begin by introducing the major technical and operational parameters and the design of the operational modes of this newly developed Ka-band millimeter-wave radar. Then, a set of measurements obtained over a period of one month at Naqu, on the Tibetan Plateau, in the summer of 2014, are analyzed to investigate the detection capability of the radar and biases from different operational modes. Finally, a cloud radar data merging algorithm is proposed to integrate the measurements from the three operational modes, and preliminary results from testing the algorithm are evaluated.

2. Major technical parameters and operational modes

The newly developed Ka-band cloud radar with a solid-state transmitter adopts Doppler radar and polarization radar technology. It works in a vertically pointing mode to obtain cloud and light precipitation vertical profiles of reflectivity Z, radial velocity $V_{\rm r}$, velocity spectrum width $S_{\rm w}$, and the depolarization factor $L_{\rm DR}$. Meanwhile, it also records Doppler spectral density data $S_{\rm z}$. The major technical and subsystem parameters are listed in Tables 1 and 2. The Ka-band is utilized in this radar to obtain as much backscattered energy as possible, while reducing the attenuation effects of air and precipitation particles. The main purpose in using the solid-state transmitter is to realize continuous measurements, since statistical results on cloud characteristics are especially important for cloud and precipitation physics. In order to improve the radar's capability for cloud measurements, three operational modes [the boundary mode (M1), the cirrus mode (M2), and the precipitation mode (M3)] are applied. Different radar pulse widths and coherent and incoherent integration techniques are used to meet the requirements for low-level and weak cloud detections. M1, with high-resolution radial velocity, is suitable for cloud observations near the surface. M2, with high sensitivity and a large minimum range, is important for weak cloud observations and radiation studies, but is unable to observe clouds and precipitation below the height of 2.1 km. M3, which does not saturate, is important to precipitation studies. It is necessary to run the three modes and combine them to observe weak clouds and precipitation from near the ground to the height of 15 km.

Table 1. Major technical parameters for the Ka-band solid-state transmitter cloud radar.

Order	Item	Technical specifications
1	Radar system	Coherent, pulsed Doppler, solid-state transmitter, pulse compression
2	Radar frequency	33.44 GHz (Ka-band)
3	Detecting parameters	Z, $V_{\rm r}$, $S_{\rm w}$, $L_{\rm DR}$, $S_{\rm z}$
4	Detection capability	⩽ −30 dBZ at 5 km
5	Range of detection	Height: 0.120–15 km Reflectivity: −50 dBZ to +30 dBZ Radial velocity: 4.67–18.67 m s^{-1} (maximum) Velocity spectrum width: 0–4 m s^{-1} (maximum) Temporal resolution: 6 s (adjustable) Height resolution: 30 m

Table 2. Subsystem parameters for cloud radar.

	Order	Item	Technical specifications
Antenna Subsystem	1	Operating frequency	Ka-band
	2	Antenna type	Cassegrain
	3	Antenna diameter	2 m
	4	Antenna gain	$\geqslant$ 53 dB
	5	Beam width	$\leqslant$ 0.35°
	6	First sidelobe level	$\leqslant$ −18 dB
	7	Sidelobe level	$\leqslant$ −40 dB
	8	Cross-polarization isolation	31.5 dB
	9	Standing wave ratio	$\leqslant$ 1.5
	10	Radar transceiver feeder	$\leqslant$ 3 dB
Transmitter subsystem	1	System	Solid-state transmitter
	2	Peak power	$\geqslant$ 50 W
	3	Duty ratio	$\geqslant$ 10%
Receiver subsystem	1	Noise Figure	$\leqslant$ 5 dB
	2	Reflectivity dynamic range	$\geqslant$ 60 dB
	3	Phase noise	$\leqslant$ −96 dBc/Hz at 1 kHz
	4	Intermediate frequency (IF) processing	Digital IF receiver
The signal processing subsystem	1	A/D bits	$\geqslant$ 14 bits
	2	Signal processing	Pulse compression, FFT, coherent integration, incoherent integration
	3	Range solution	30 m
	4	Number of range gates	$\geqslant$ 500
	5	Output	Doppler spectral density data

The major parameters that affect the radar's capability of detection include the number of range gates (Num_gate), the range sample volume spacing (R_space), the maximum range (R_max), the minimum range (R_min), the pulse width (τ), the pulse repetition frequency (PRF), the number of coherent integrations ($N_{\rm coh}$), the number of incoherent integrations ($N_{\rm ncoh}$), the number of fast Fourier transform (FFT) points ($N_{\rm FFT}$), and the radial velocity resolution (ΔV). With application of coherent integration, the maximum range is inversely proportional to the PRF. The Nyquist velocity can be expressed as

$$V_{\max}=\frac{\lambda \mathrm{PRF}}{4N_{\rm Coh}}\ , \tag{1}$$

where λ is the wavelength. In this way, despite the fact that the PRF is the same in all of the three operational modes, the Nyquist velocity for the three modes still changes in response to the different numbers of coherent integrations. Another parameter related to radial velocity is the velocity resolution. For cloud radar that works in the vertically pointing mode, the radial velocity is closely related to the air vertical motion. Thus, its requirement for velocity resolution is much higher than that of weather radar. The relation between velocity resolution, the Nyquist velocity and the number of FFT points can be written as

$$\Delta V=\frac{V_{\max}}{N_{\rm FFT}}\ . \tag{2}$$

The operational modes are categorized into two types: the narrow pulse width modes, which include boundary mode M1 and precipitation mode M3; and the wide pulse width mode, which is represented by the cirrus mode M2 (the major operational parameters are given in Table 3). M1 and M3 are mainly used for measurements of clouds and light precipitation in the mid and lower levels. The minimum ranges are relatively small for these two modes, while the minimum detectable reflectivities are large. The major difference between the two modes is that four times the number of coherent integrations is performed for M1, which reduces the minimum detectable reflectivity by 6 dB. Meanwhile, the Nyquist velocity decreases four-fold, while the radial velocity resolution increases four-fold. M2 is applied for cloud detections in the mid and upper levels, where clouds are characterized by high altitude, small reflectivity, and weak vertical motion. For these reasons, a frequency modulation pulse waveform, with large pulse width, is used in M2, which has a relatively large minimum range but a small minimum detectable reflectivity. Based on the numbers of coherent and incoherent integrations, it is known that dwell time for the three operational modes (i.e., the time to obtain a radial measurement) is 2 s. Thereby, one cycle of the three operational modes will take 6 s, and 600 radial measurements can be obtained within a period of 1 h. One mode alternates with another during cloud radar observation. Once the radial measurement is finished in one mode, the radar immediately switches to another mode. The observations collected by the three different modes are saved separately and eventually the merged radar data are produced.

Table 3. Major operational parameters for the three operational modes.

Term	Boundary mode (M1)	Cirrus mode (M2)	Precipitation mode (M3)
τ	0.2 µs	12 µs	0.2 µs
PRF	8333 Hz	8333 Hz	8333 Hz
$N_{\rm coh}$	4	2	1
$N_{\rm ncoh}$	16	32	64
$N_{\rm FFT}$	256	256	256
Dwell time	2 s	2 s	2 s
Num_gate	256, 128	512, 256	512, 256
R_space	30 m	30 m	30 m
R_min	30 m (theoretical); 120 m (practical)	1800 m (theoretical); 2010 m (practical)	30 m (theoretical); 120 m (practical)
R_max	18 km	18 km	18 km
$V_{\rm max}$	4.67 m s^{-1}	9.34 m s^{-1}	18.67 m s^{-1}
V	0.018 m s^{-1}	0.036 m s^{-1}	0.073 m s^{-1}
Minimum detectable reflectivity (5 km)	−24 dBZ at 5 km	−38 dBZ at 5 km	−18 dBZ at 5 km

3. Evaluation of the different operational modes

Cloud radar data for cloud and precipitation observations at Naqu [(31.48°N, 92.01°E); 4507 m], on the Tibetan Plateau, were used to evaluate the data quality observed by the three operational modes. The measurement period was from 1 July to 31 August 2014. Continuous cloud radar observations over a period of one month from 5 July to 4 August were obtained and used for statistical analysis to investigate the capability of radar detection.

3.1. *Minimum detectable reflectivity*

Using the valid cloud radar measurements (greater than the specified SNR threshold of −12 dB), we obtained the minimum detectable reflectivity and their variations with height for the three modes (Fig. 1), based on statistics of minimum reflectivity at different heights. The results showed that, for M1, M2 and M3, the minimum reflectivities at 5 km were −23.9 dBZ, −37.7 dBZ and −17.9 dBZ respectively, which were highly consistent with the calibration test results of −24.0 dBZ, −38.0 dBZ and −18.0 dBZ. The minimum detectable reflectivities of the three modes were mainly related to pulse compressions and the number of coherent integrations. Compared with M3, four times as many coherent integrations were performed for M1, and the minimum detectable reflectivity reduced by 6 dB [10log4]. Similarly, twice as many coherent integrations were performed for M2, and the pulse compression ratio was 60; theoretically, the minimum detectable reflectivity can reduce by 20.8 dB [10log(2×60)].

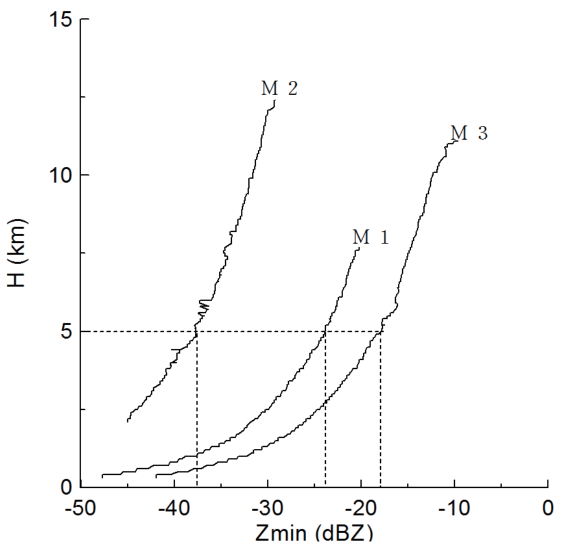

Fig. 1. Changes in minimum detectable reflectivity (x-axis) with height (y-axis) for the three operational modes (labeled). The dashed lines show the minimum detectable reflectivities at 5 km.

3.2. *Measurement consistency*

Probability distributions of reflectivity from the three modes were calculated using the month's measurements. Considering the fact that M2 has a large minimum range, in which only measurements from M1 and M3 are available, we only used measurements beyond the minimum range of M2. Figure 2a shows the number of occurrences of reflectivity measured simultaneously by the three modes. Note that the number of samples used in Fig. 2a is the same for all of the three modes. Figure 2b presents the number of occurrences of reflectivity measured independently by each mode, and the numbers of measurements from these modes are different. Since no pulse compression and coherent integrations are performed for M3, this mode has the most accurate reflectivity data moments. For this reason, we compared results from the other two modes with those from the M3 mode. Figure 2a shows clearly that the patterns of the number of occurrences of reflectivity from the three modes were quite similar, but certain displacements existed. For M1, the number-of-occurrence curve for reflectivity less than 5 dB shifted to the right with a displacement of about 1 dB. That is, the M1 mode overestimated the reflectivity by 1 dB. For reflectivity larger than 5 dB, the M1 mode underestimated the reflectivity by about 2 dB; and in this case, the benefit of coherent integration for M1 was less than the theoretical value.

Fast fluctuations of the returns from hydrometeors can make a mess of coherent integration. Such a situation often happens for measurements of convective precipitation below the zero-temperature level, since the gain of reflectivity from coherent integration becomes less significant due to the small scale of convective cloud, large terminal velocity and strong atmospheric turbulence. For the M2 mode, the number-of-occurrence of reflectivity agreed very well with that from M1 and M3, but M2 overestimated the reflectivity by 2 dB. Figure 2b shows that, for strong reflectivity larger than -10 dBZ, the number of occurrences of reflectivity within the three modes agreed very well with the results in Fig. 2a, because the reflectivity stronger than -10 dBZ below 12 km could be observed by the three modes (Fig. 1). For weak reflectivity less than -10 dBZ, the number-of-occurrence curves changed significantly. The number-of-occurrence of weak reflectivity greatly increased in the measurements from the highly sensitive M2 mode. The M1 and M3 modes seldom measured reflectivity less than -30 dBZ.

In order to further analyze the reflectivity biases, we present the two-dimensional number of occurrences of reflectivity measured by the three modes (Fig. 3). High occurrences of reflectivity occurred below the diagonal for the M1 and M3 modes, with a displacement of about 1 dB (Fig. 3a), and the M1 mode overestimated the reflectivity by about 1dB. However, in the area with strong reflectivity, the occurrence distribution pattern shifted away from the diagonal and the M1 mode sometimes underestimated the reflectivity. This result further confirms the phenomena shown in Fig. 2. The two-dimensional number of occurrences of reflectivity from the M2 and M3 modes indicate that the high occurrence area occurred below the diagonal with a displacement of 2dB, and parallel to the diagonal, suggesting that the reflectivity obtained from the M2 mode was larger than that from the M3 mode by 2 dB. Furthermore, such systematic biases will not change with an increase or decrease in reflectivity.

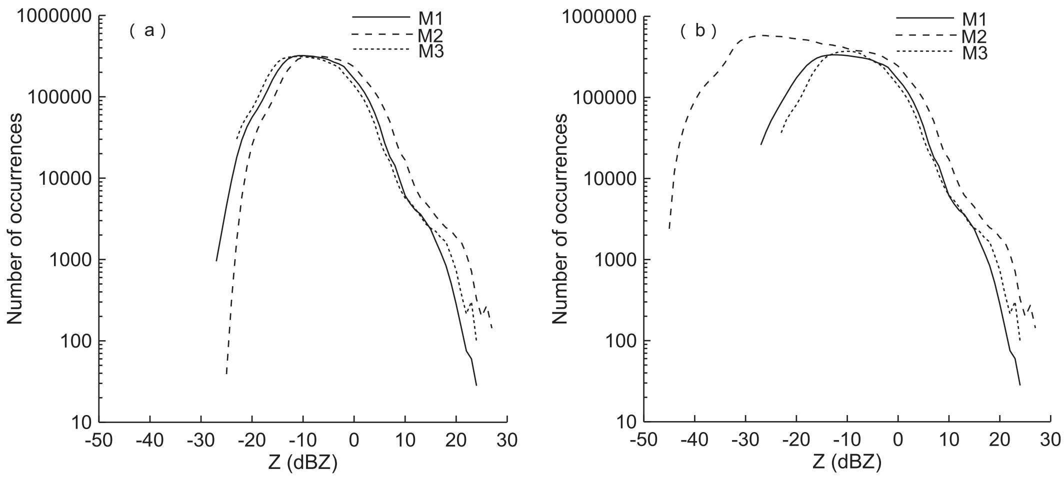

Fig. 2. Numberofoccurrences of reflectivity obtained by the three modes: (a) reflectivity measured simultaneously by the three modes beyond the minimum range of M2; (b) all measurements obtained independently by each operational mode.

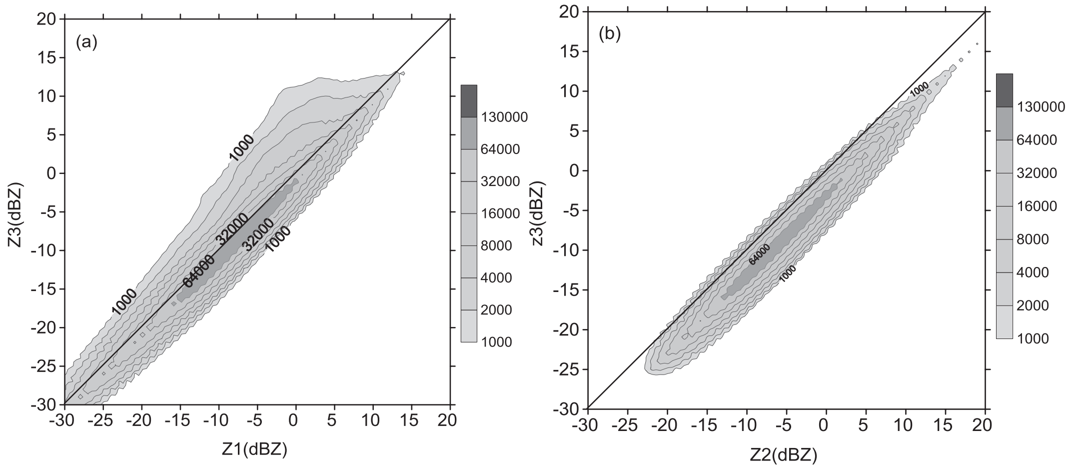

Fig. 3. Two-dimensional number-of-occurrences of reflectivity for (a) M1 and M3 and (b) M2 and M3. Z1, Z2 and Z3 represent the reflectivity from the M1, M2 and M3 modes, respectively.

Figure 4 explains the relationship between the averaged biases of reflectivity by M1 and M3 and S_w. The coherent integration underestimated reflectivity when S_w was greater than 0.55 m s^{-1}. The bias of reflectivity between the two modes reached −2.0 dB when S_w was 0.85 m s^{-1}. The biases of reflectivity measurements between M1 and M3 indicate that the coherent integration with fast moving hydrometeors (large precipitation particles) as targets is contributing to some of the poor performance of the M1 mode. The number of occurrences of the radial velocity (positive values represent upward motion), L_{DR}, and velocity spectrum width obtained by the three modes are shown in Fig. 5. The M1 mode gave the minimum V_{max} (4.67 m s^{-1}), while M3 obtained the largest V_{max} (18.67 m s^{-1}). In order to eliminate the impacts of velocity aliasing, we used the radial velocity obtained by the M3 mode to evaluate the possibility of velocity aliasing in the measurements from the M1 and M2 modes. The results shown in Fig. 5a are from radial velocity samples in which the absolute values of radial velocity obtained by the M3 mode were less than the V_{max} of the M1 mode. Since the M2 and M3 Nyquist velocities are large, there is little possibility for the occurrence of velocity aliasing. As a result, the radial velocities measured by the two modes agreed very well. The number of occurrences of radial velocities obtained by the M1 mode were also consistent with those by the other two modes when the absolute values of the radial velocities were smaller than 3.5 m s^{-1}. However, when the absolute values of the radial velocities were large, the number of occurrences of positive radial velocities increased, whereas the number of occurrences of negative radial velocities decreased. This was particularly distinct when the velocities were near the range of ±4.0 m s^{-1}. That is, part of negative radial velocities with the M1 mode "jump" to positive radial velocities. This phenomenon may be attributable to the fact that precipitation particles of various sizes exist within the target object; the fall speeds of particles increase with size, which work together with turbulence and result in a wide interval distribution of the Doppler spectral density within the target object. Although the radar radial velocity observed by cloud

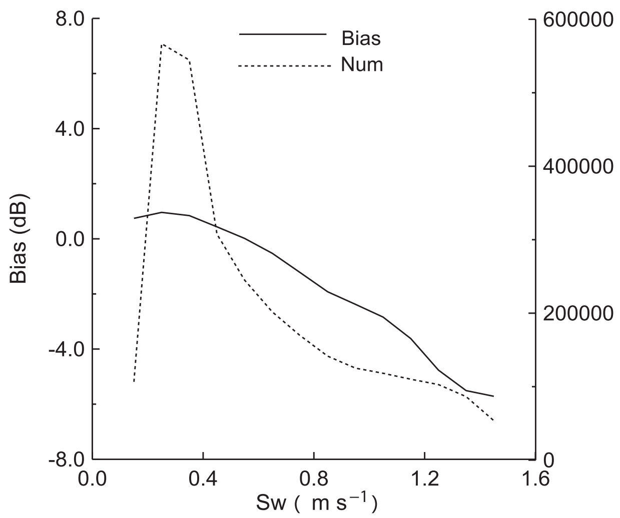

Fig. 4. Variation of averaged bias of reflectivity by M1 and M3 (solid line), and the number of samples with velocity spectrum width (dashed line).

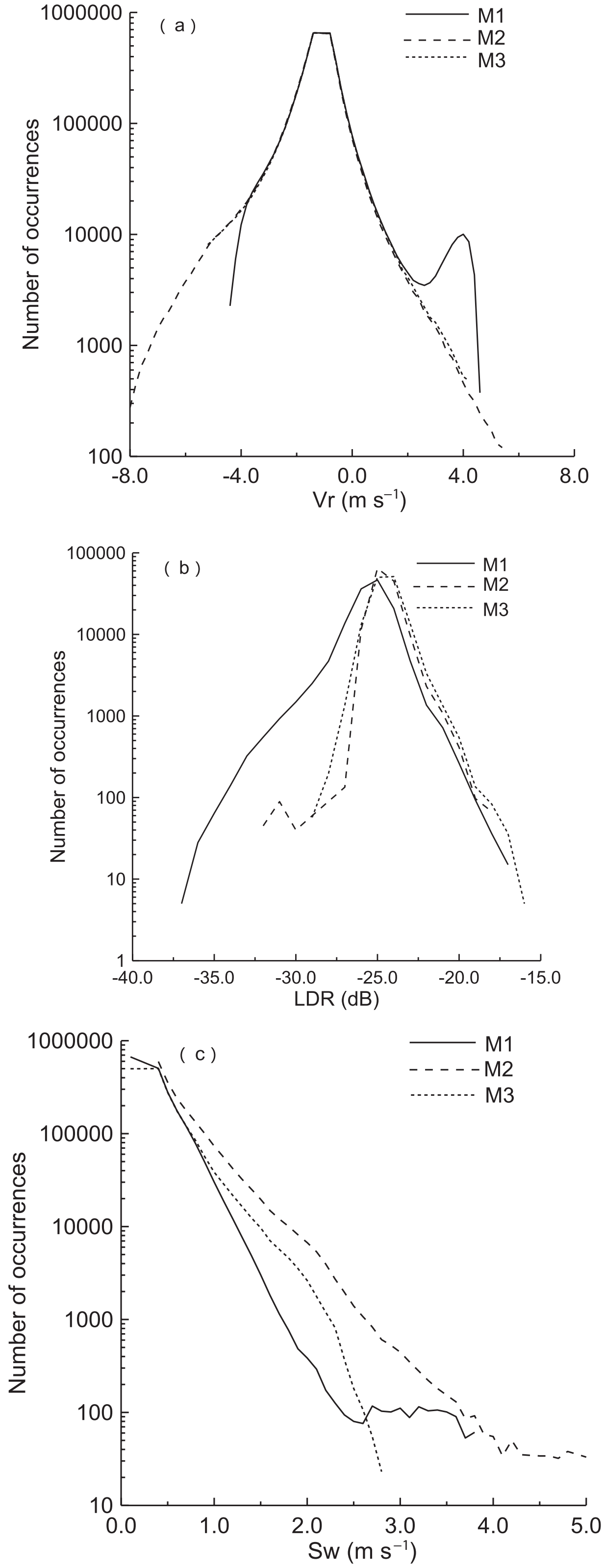

Fig. 5. As in Fig. 2a, but for the (a) radial velocity, (b) L_{DR} and (c) velocity spectrum width obtained by the different modes.

radar was not larger than the V_{max} of M1, part of the Doppler spectral density corresponding to negative radial velocity exceeded the V_{max} of M1. As a result, aliasing happened to part of the Doppler spectral density data and some negative radial velocities that corresponded to large precipitation particles became positive. Integration of the aliasing of the Doppler spectral density data observed by M1 will lead to bias in radial velocity and some negative radial velocities of −4.0 m s^{-1} becoming positive. The reasons are explained in the following (Figs. 6 and 7). For the M2 and M3 modes, with large V_{max}, there is little chance of aliasing happening for Doppler spectral density data. For this reason, we only used those

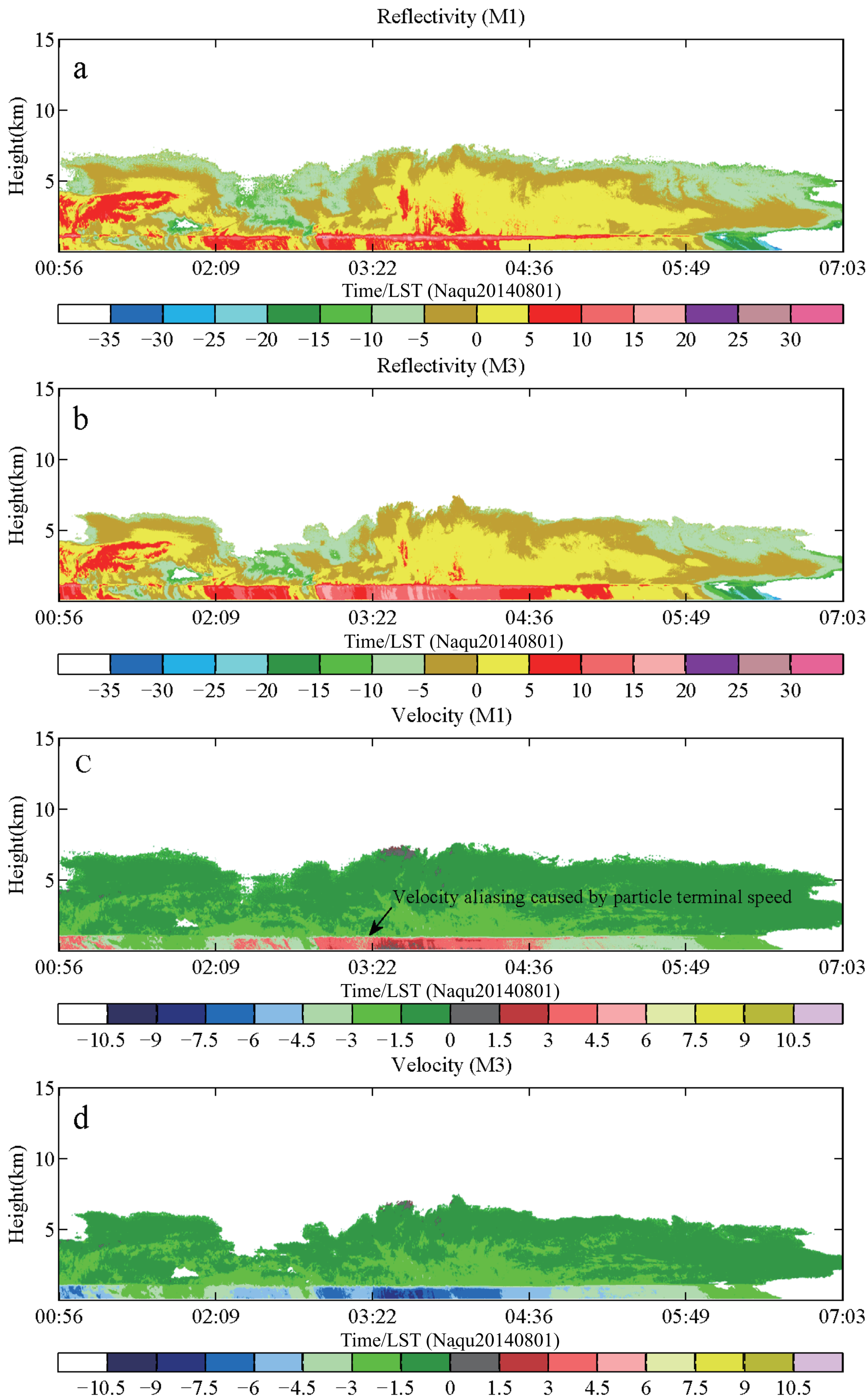

Fig. 6. Time–height cross sections of reflectivity and radial velocity measurements from M1 and M3 for 1 August 2014: (a, b) measurements from the M1 mode; (c, d) measurements from the M3 mode. The height is AGL.

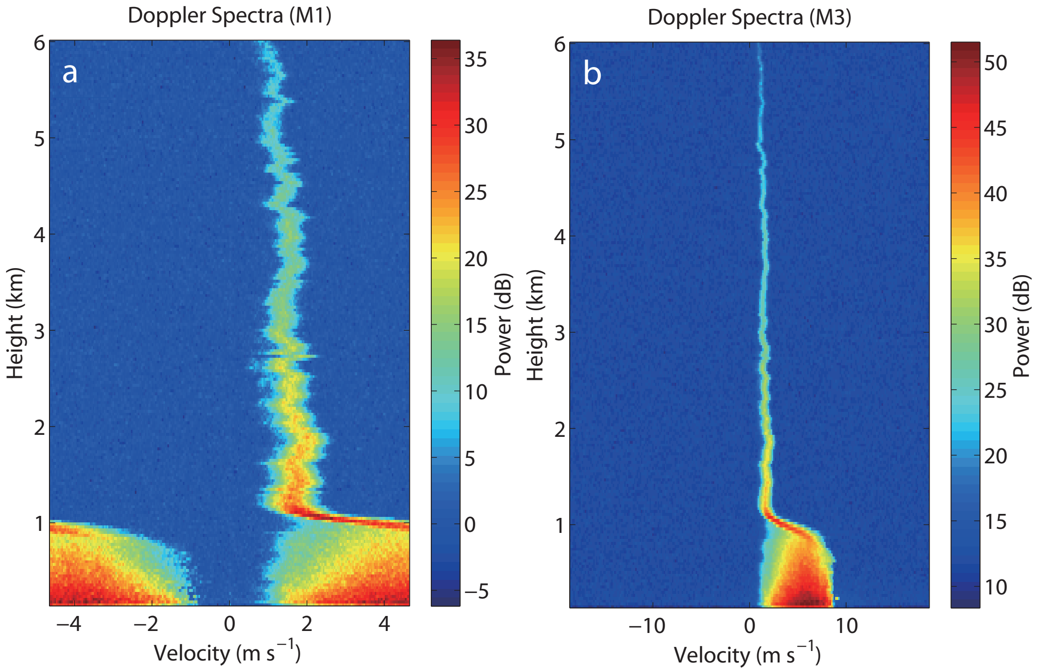

Fig. 7. Doppler spectral density at different heights at 0436 LST (LST=UTC+8) 1 August 2014 observed by the (a) M1 mode and (b) M3 mode.

high-resolution velocities obtained by the M1 mode with absolute values smaller than 3.5 m s^{-1} for the merging process. Generally, the agreement in radial velocities obtained by the three modes was better than that of reflectivity. However, the impacts of the partial aliasing in the Doppler spectral density data from the M1 mode cannot be ignored.

The L_{DR} observed by the cloud radar with cross-polarization isolation for antenna of 31.5 dB shows that the number-of-occurrence distribution curves from the three modes were consistent when L_{DR} was greater than −25 dB (Fig. 5b). However, for other L_{DR} values, the number-of-occurrence distributions for the M1 mode were different to those for the other two modes. The M1 mode provided the minimum L_{DR}, followed by the M2 mode, and the M3 mode gave the largest value. This is mainly because coherent integration has different impacts on signals with different SNRs. The co-polar reflectivity is much larger than the cross-polar measurements. As a result, the coherence of co-polar echo signals was better than the cross-polar signals. Thereby, co-polar reflectivity can benefit more from coherence integration than that observed in the cross-polar channel. L_{DR} is underestimated by coherent integration. The smaller the L_{DR} is, the more severe the underestimation will be.

Certain biases existed in the velocity spectrum width obtained by the different modes (Fig. 5c), which are attributable to the effects of coherent and incoherent integrations and sidelobes from the pulse compression. Compared with the M3 mode, the M1 mode underestimated the velocity spectrum width due to the influence of coherent integration, while the M2 mode overestimated the velocity spectrum width due to the effects of sidelobes from the pulse compression.

In order to explain the reasons for velocity aliasing by M1, Fig. 6 shows time–height cross sections of reflectivity, radial velocity (positive upward) for 1 August 2014 observed by M1 and M3. The vertical *y*-axis indicates height above ground level (AGL), the *x*-axis indicates local standard time (LST), and the origin indicates the radar antenna (4560 m AGL, the same hereafter). Figure 7 presents profiles of Doppler spectral density by the M1 and M3 modes. The M1 mode observed positive velocity and M3 mode observed negative velocity with reflectivity stronger than 5 dBZ below the bright band (1.2 km) in the area marked with arrow in Fig. 6. We found Doppler spectral density aliasing below 1.2 km (Fig. 7), which was the reason for the positive velocity observed by M1.

3.3. *Hydrometeor detection*

To assess the importance of the enhanced sensitivity caused by pulse compression and coherent integration in M2 relative to M1 and M3, we compared the hydrometeor detections produced by M1 and M3 with those by M2. We defined the undetected rate of reflectivity for the M1 and M3 modes relative to M2 as the ratio between the numbers of valid observations that could be obtained by the high-sensitivity mode (M2) but could not be obtained by the low-sensitivity modes (M1 or M3), and the total numbers of valid observations obtained by the high-sensitivity mode (M2) at a certain height. A smaller undetected rate indicated a higher capability of detection. At the levels below the minimum range of the M2 mode, the undetected rate of the M3 mode was calculated using the measurements from the M1 mode as reference; above this level, the undetected rates for M1 and M3 were calcu-

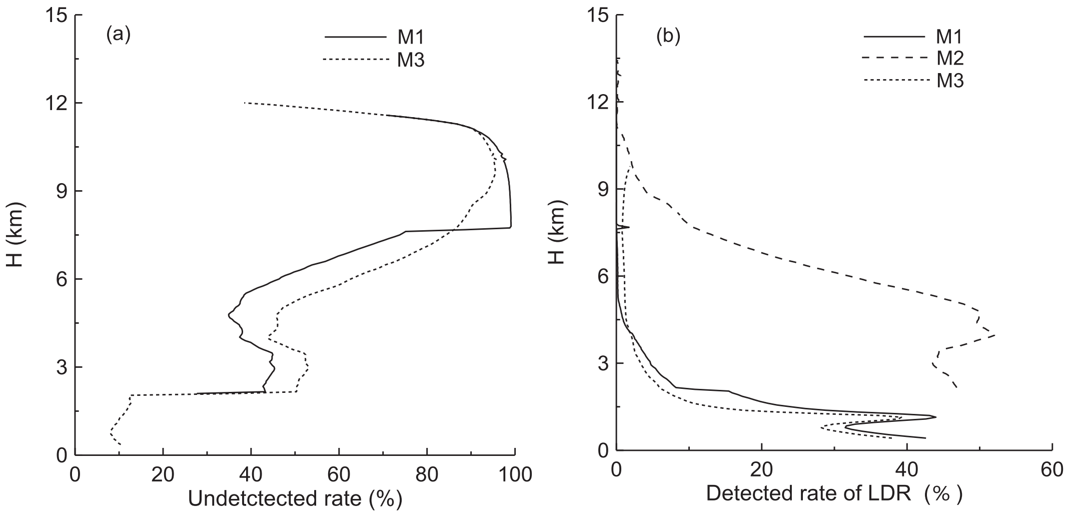

Fig. 8. The (a) undetected rate of reflectivity for the M1 and M3 modes relative to M2, and (b) the detection rate of L_{DR}.

lated using the data from the M2 mode as reference. Figure 8a depicts the undetected rates of the M1 and M3 modes at different heights. Below 2.01 km (the minimum range of M2), about 10% of the hydrometers were missed by M3 relative to M1, due to the minimum detectable reflectivity for M3 being 6 dB higher than that of M1. Compared with M2, at least 50% of mid-tropospheric cloud data were missing in the observations by M1 and M3, and the undetected number increased with height. At 6 km, M1 and M3 could only obtain about 20%–40% of the hydrometers. Apparently, the cloud radar can observe different cloud tops and bases in different modes. The vertical distributions of the missed hydrometeor detections illustrate that hydrometeors above approximately 4.5 km create the largest problems for these two less-sensitive modes. These findings indicate that it is difficult for the cloud radar in the M1 and M3 modes to observe clouds over 5 km. High radar sensitivity provided by the pulse compression and coherent integration techniques is critical to developing comprehensively accurate depictions of hydrometeors in a vertical column of the atmosphere.

For L_{DR}, the cross-polar reflectivity is much smaller than that in the co-polar channel. In many cases, co-polar reflectivities are stronger than the minimum detectable reflectivity, but the cross-polar reflectivities are smaller than the minimum detectable reflectivity. In this case, the L_{DR} cannot be obtained. The L_{DR} detection rate was defined as the ratio between the total number of L_{DR} observations and the total number of co-polar reflectivity observations at each level. Figure 8b indicates that the L_{DR} detection rates for M1 and M3 were not larger than 50%, even at the lower levels. At 1 km, the rate reduced to 30%. At 1.4 km, the L_{DR} detection rate increased to 45%, due to the increase in L_{DR} and reflectivity at around the zero-temperature level. At 3 km, the L_{DR} detection rate was already very low. Similarly, the L_{DR} detection rate for the M2 mode also decreased with height. At 2.1 km, the L_{DR} detection rate for the M2 mode was higher than that for the M1 mode by about 40%. In general, the cloud radar detected most of the L_{DR} of clouds and precipitation below 5km. The most difficult L_{DR} to detect occurred above 5 km.

These results provide a basis for merging the measurements of the three modes. The pulse compression and coherent integration techniques are critical to improving the cloud radar capability of detection.

4. Merging algorithm for the radar data obtained by the three modes

4.1. *Principles of cloud radar data from the different modes*

The M1 mode has high sensitivity and velocity resolution for observing boundary layer clouds, which are often composed of small droplets. M2 has the highest available sensitivity and a large minimum range, which is suitable for observing weak reflectivity and high-altitude clouds. The M3 mode has a large Nyquist velocity, a large maximum reflectivity and a low minimum range, which is suitable for observing light precipitation. To develop a complete picture of the vertical distribution of hydrometeors, we must integrate the data from the three modes. The following are several key issues in the implementation of the merging process:

(1) Reliability of the data. Only when the SNR exceeds a certain threshold can the cloud radar observe high-quality measurements of reflectivity, radial velocity and velocity spectrum width. Conversely, when the SNR is very small, large biases exist in the radar data.

(2) Over-saturation problem. The dynamic range of the cloud radar is about 60 dB. Once the reflectivity is beyond the range, biases will occur in the measurements. In particular, the L_{DR} value will be overestimated.

(3) Radial velocity aliasing. When large particles or

strong vertical motions exist, coherent integration will lead to radial velocity aliasing for the M1 and M2 modes. The $V_{\max}$ for the M3 mode is 18.67 m s^{-1}. For vertically pointing radar, velocity aliasing seldom happens for the M3 mode.

(4) Radial velocity resolution. The resolution is the highest for M1 and lowest for M3. High-resolution data should be used when other parameters meet requirements.

(5) Biases in the measurements from different modes.

Based on the above considerations, the principles of the merging process are: (1) when radial velocity aliasing occurs, try to use data from the M3 mode, which provides the largest Nyquist radial velocity; (2) when reflectivity saturation occurs, try to use data from the low-sensitivity modes M1 and M3; (3) it is better to use data with high radial velocity resolution (i.e. data form M1 mode) when no aliasing and saturation occur for M1; (4) when the SNR is large enough for the other modes, avoid using data from M2; (5) reflectivity, radial velocity and velocity spectrum width should be from the same mode; (6) a separate algorithm should be implemented for merging L_{DR} data.

4.2. *Merging reflectivity, radial velocity and velocity spectrum width*

The steps for merging reflectivity, radial velocity and velocity spectrum width include:

(1) Delete the data below a defined SNR threshold (−12 dB; the Doppler spectrum estimation is used in the data processor in the cloud radar) and all of the data below the corresponding minimum range. The defined SNR threshold was calculated based on statistical results.

(2) Correct the systematic bias of reflectivity. Using systematic bias analysis for each operational mode, the reflectivity obtained by the M2 mode will be corrected (−2 dB from the observed reflectivity).

(3) Merge data below the minimum range of the M2 mode. Only measurements from M1 and M3 are available in this case. The $V_{\max}$, SNR and over-saturation of reflectivity from the M1 mode are utilized as criteria to determine which mode is used. The minimum detectable reflectivity for the M1 mode plus the dynamic range of reflectivity can be regarded as the maximum detectable reflectivity for the M1 mode. If the reflectivity obtained by the M3 mode is larger than the maximum reflectivity from the M1 mode, data from the M3 mode should be used. If the M3 velocity does exceed the M1 Nyquist velocity and the M3 data SNR is greater than −2 dB (10 dB greater than the minimum detectable reflectivity), we use M3 data. In other cases, data from the M1 mode should be used.

(4) Merge data above the minimum range of the M2 mode. Within this range, data from all of the three modes are available. When over-saturation occurs in the reflectivity from the M1 mode, M3 mode data should be used. When over saturation occurs in the reflectivity from the M2 mode, M1 mode data should be used. If the M3 velocity does exceed the M2 Nyquist velocity and the M3 data SNR is greater than −2 dB, we use M3 data. If the M2 velocity does not exceed the M1 Nyquist velocity and the M1 data SNR is greater than −2 dB, we use M1 data. In other cases, data from the M2 mode should be used.

4.3. *Merging* L_{DR}

Note that the cross-polar reflectivity is much smaller than the co-polar reflectivity. In many cases the radar can obtain valid measurements of the other three variables but cannot obtain valid L_{DR} data. Thereby, merging L_{DR} must be done separately. Two factors must be considered when merging L_{DR}: one is the over-saturation of co-polar reflectivity from the high-sensitivity operational mode; and the other is whether the data from the low-sensitivity mode are valid. Thereby, the principle for merging L_{DR} is that, under the premise of avoiding over-saturation, try to use data obtained by the mode with a high SNR.

(1) Merging data above the minimum range of the M2 mode. If the M3 reflectivity exceeds the maximum reflectivity observed by the M1 mode, we use M3 L_{DR}. Otherwise, we use M1 L_{DR}.

(2) Merging data above the minimum range of the M2 mode, If the M3 reflectivity exceeds the M1 maximum reflectivity, we use M3 L_{DR}. If the M1 reflectivity exceeds the M2 maximum reflectivity, we use M1 L_{DR}. In other cases, M2 L_{DR} is used.

5. Cloud radar observation and merged results

Based on the radar measurements during the time period of 5 July to 4 August 2014, we analyzed the number of occurrences of merged valid reflectivity, the mode usages and the merged results, compared with the three modes. The dwell time of radial measurement for each operational mode is 2 s. One cyclic measurement by all three modes takes 6 s. Thereby, each operational mode can obtain 24×600 radial data in one day, and the total radial data number for one month is 432 000. The vertical distributions of the number of occurrences of valid merged reflectivity are illustrated in Fig. 9a. The results indicate that the clouds over the Tibetan Plateau were largely distributed above 6 km and below 4 km. Low-level clouds and precipitation events near the surface occurred the most frequently. The largest number of occurrences of cloud detection was found at 3 km, which accounted for 42% of the total radial data. Another layer of large cloud cover appeared above 7 km, where the number of occurrences of cloud detection accounted for 33% of the total. The number of occurrences of cloud detection was low below 2.01 km, because only measurements from the low-sensitivity modes of M1 and M3 were available. Figure 9b shows the percentage contributions of M1, M2 and M3 to the merged cloud masks. The percentage contributions of M1 and M3 were similar below 1 km, but the usage of the M1 data increased with the increase in height. Within the height range of 1–2 km, more data from the M1 mode were used, while within the range of 2.1–6 km most of the merged data were from

M1 and M2 and the contribution of M3 data was less than 10%. Above this height, more M2 data were used. The M3 data were used during precipitation events below the zero-temperature level; the M1 data detected clouds with moderate reflectivity between 1.2 and 6 km; and the M2 data were used for the remaining, weaker reflecting hydrometeors over 6 km.

Further analysis of the proportion of radial velocity aliasing in the total radial velocity obtained in the M1 mode and the proportions of reflectivity over-saturated in the M1 and M2 modes (Fig. 10) suggested that aliasing M1 radial velocity occurred most frequently below 1.5 km, where 50% of the radial velocity aliased. At levels above 1.5 km, the proportion of aliasing radial velocity rapidly decreased and the proportion was only 5% at 2.2 km. Such a distribution pattern of radial velocity aliasing is related to the fact that the zero-temperature level over the Tibetan Plateau is located at 1.4 km, where solid-form precipitation particles start melting. The falling speeds of these melting particles increase rapidly, leading to large radial velocities that are beyond the M1 Nyquist velocity (Fig. 10a). The distribution of over-saturation indicated that, for the M1 mode, most of the over-saturation occurred below 1 km, and the proportion of over-saturation was only 6% at 0.3 km. For the M2 mode, over-saturation occurred at 2.1 km and accounted for 1.2% of the total measurements (Fig. 10b). The above reasons indicate that the low M1 Nyquist velocity is the major reason that limits the application of M1 data in merged data. Over-saturation for M1 and M2 basically had little impact on the detection results.

Figure 11 presents time–height cross sections of reflectivity and radial velocity on 8 July 2014, observed by the

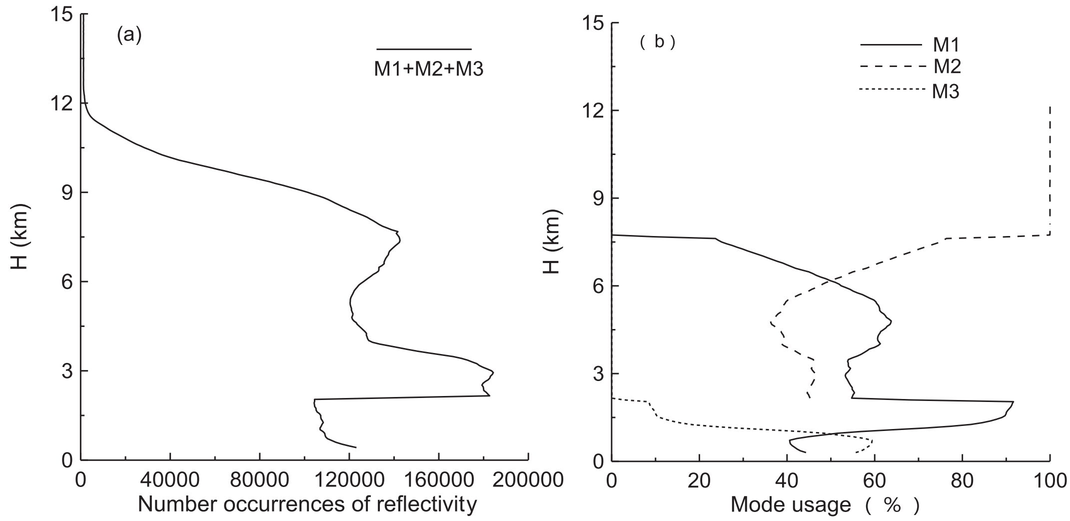

Fig. 9. The (a) number of occurrences of valid merged reflectivity by cloud radar at different height levels, and (b) percentage contributions of M1, M2 and M3 to the merged cloud mask.

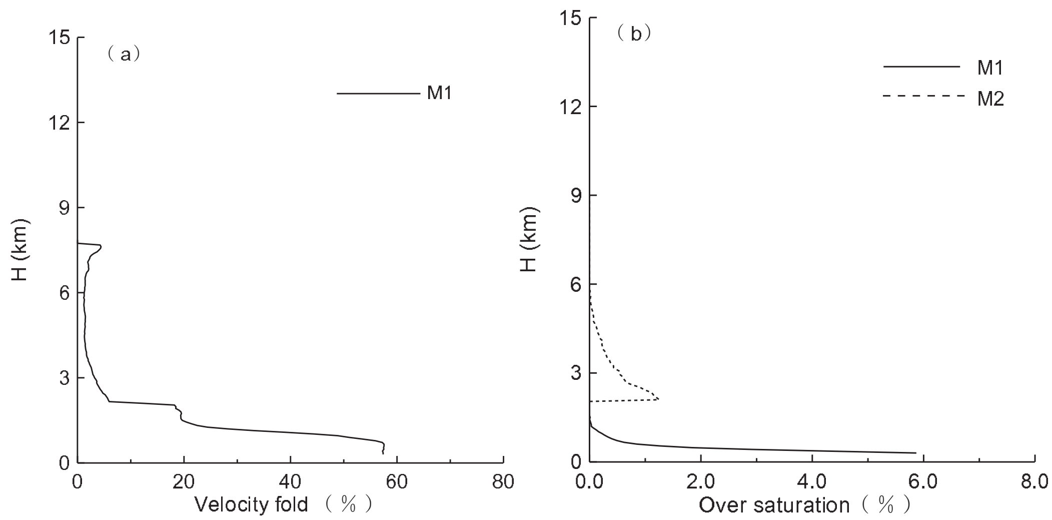

Fig. 10. The (a) proportion of radial velocity aliased in the total radial velocity obtained from the M1 mode, and (b) proportion of reflectivity over-saturated in measurements from the M1 and M2 modes.

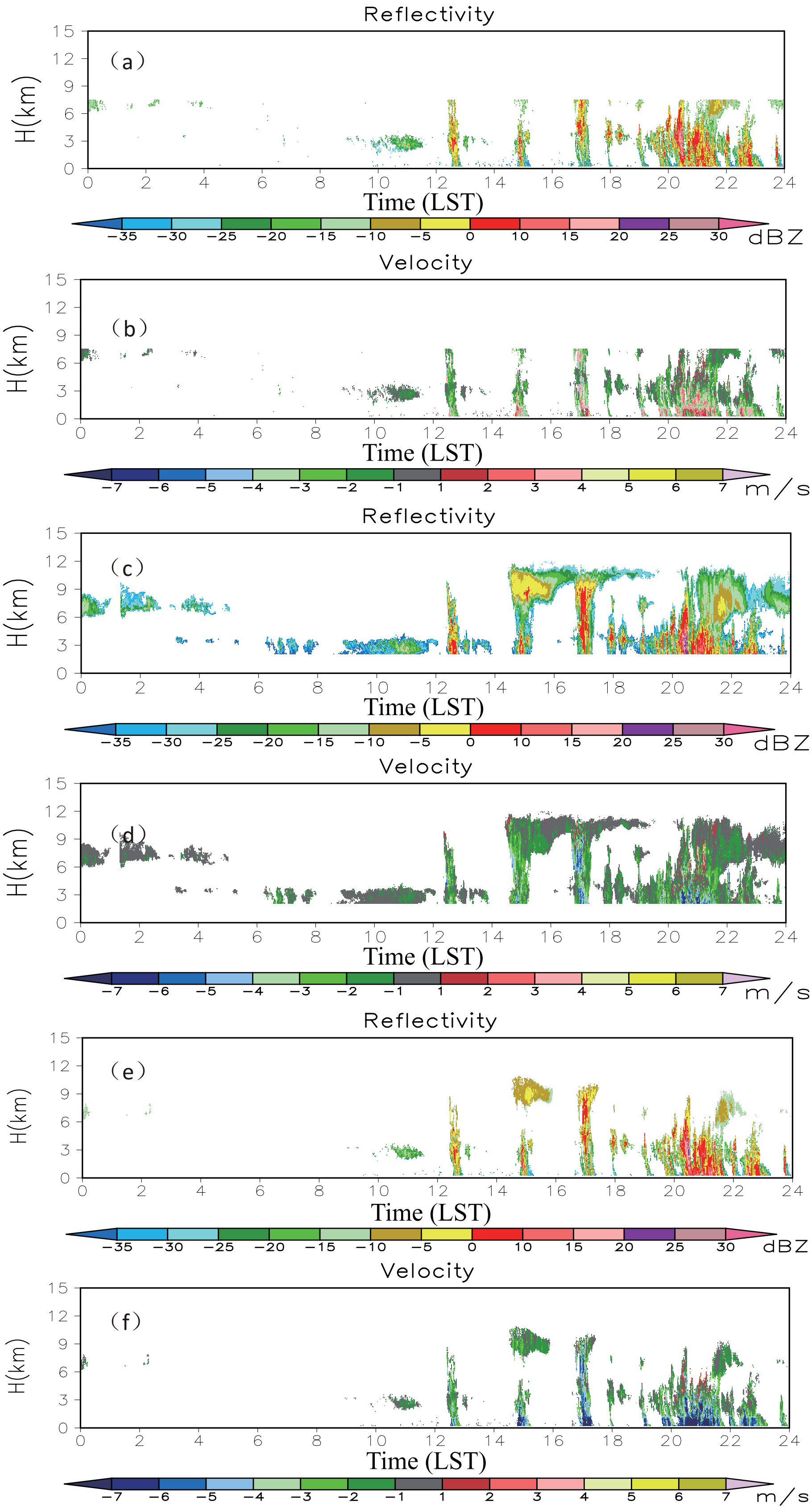

Fig. 11. Time–height cross sections of reflectivity and radial velocity measurements from the three operational modes for 8 July 2014: (a, b) measurements from the M1 mode; (c, d) measurements from the M2 mode; (e, f) measurements from the M3 mode. The height is AGL.

cloud radar in the three modes. High-level clouds above 6 km and mid-level clouds at around 3 km formed after the deep convection dissipated at around dawn (0658 LST). Surface heating resulted in convective cloud developments after 1000 LST. After 1200 LST, convective cloud cells were still in their developing stages when they passed over the radar station; the cloud top was at 12 km, where anvil clouds formed. After 2000 LST, the convective clouds reached their mature stage, with a large horizontal scale and high top. Comparing the reflectivity from the M2 mode (Fig. 11c) with that from the other two modes (Figs. 11a and e), only the M1 and M3 data were available below 2.01 km. The M2 mode obtained high clouds between 6–9 km and mid-level clouds at 3 km during the period 0000–1000 LST. The M1 and M3 modes only captured a small part of the clouds, and the cloud structures and cloud boundaries from the two modes were far from satisfactory. The greater M2 reflectivity values compared with the M3 data within a cloud at 1500 LST and 10 km possibly resulted from pulse compression sidelobes or reflectivity biases between M2 and M3. The M3 velocity data were negative in the lower part of the convective clouds, which was actually the downward radial velocity caused by the falling of precipitation particles. A large proportion of these negative velocities exceeded the M1 Nyquist velocity of 4.67 m s^{-1}. Note that the M1 radial velocity data were positive at the same time, indicating that these radial velocity data were aliased. Velocity aliasing of solid precipitation particles did not occur above 1.5 km.

Figure 12 shows the merged reflectivity, radial velocity, spectrum width and L_{DR} from the merged data on 8 July 2014. The M1 and M3 data were used below 2.01 km, while reflectivity larger than 5 dBZ was mainly from the M3. The merged radial velocity data were not aliased. Above 2.01 km, most of the merged data were from the M2 mode. The merged cloud structures of reflectivity and radial velocity were reasonable. However, a distinct boundary appeared at 2

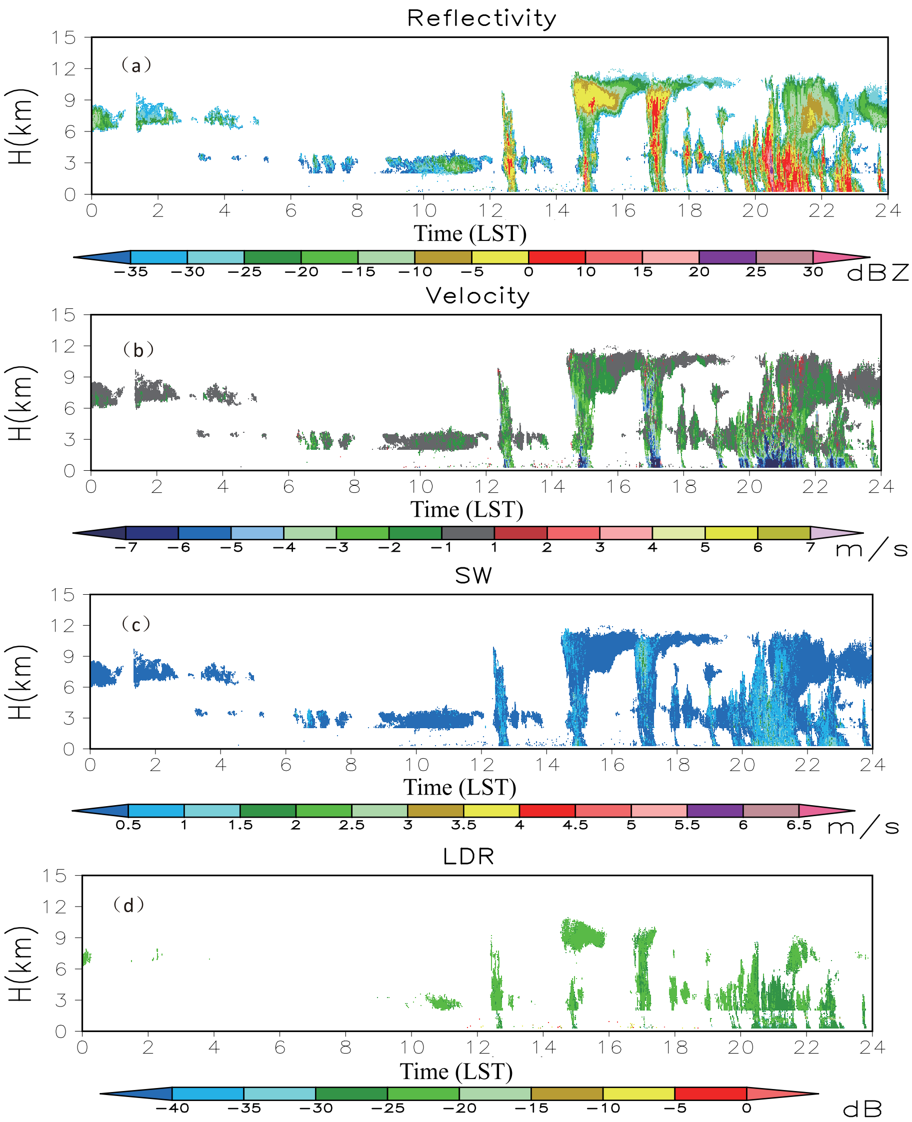

Fig. 12. Time–height cross sections of (a) reflectivity, (b) radial velocity, (c) spectrum width and (d) L_{DR}, from the merged data for 8 July 2014.

km, due to the different sensitivities among the three modes. The velocity spectrum widths were greater than 2 m s^{-1}, due to large precipitation particles and strong turbulences within convective clouds at the developing stage, while the velocity spectrum widths were small in the anvil clouds. L_{DR} values were large and reached up to −15 dB at 1.5 km within the bright band between 2030 and 2300 LST. Large velocity values were also observed in the bright band. For other snow/ice and liquid clouds and precipitation, L_{DR} values ranged between −20 and −30 dB.

6. Conclusions

The Third Tibetan Plateau Atmospheric Science Experiment was carried out during 1 July to 31 August 2014. A Ka-band solid-state transmitter cloud Radar was deployed at Naqu, on the Tibetan Plateau, for observation of the vertical structure of clouds and light precipitation. In this paper, we first introduce the major technical parameters of the cloud radar and the design of the three operational modes. The minimum detectable reflectivity, number of occurrences of valid measurements for three operational modes, and bias in the measurements for each operational mode, are also introduced. A merging algorithm for reflectivity, radial velocity, spectrum width and L_{DR} from the three modes is then proposed and the results analyzed. The major conclusions are as follows:

(1) This cloud radar, with a solid-state transmitter, adopts three operational modes with different pulse widths and coherent and incoherent integrations. The minimum detectable reflectivity of −35 dBZ at 5 km and the minimum detection range of 0.2 km are realized through merging measurements from the three modes. The range of detectable reflectivity is expanded to meet the requirements for cloud and precipitation observations. The minimum detectable reflectivities for the three modes are consistent with theoretical results.

(2) Compared with the M1 mode, the M3 mode underestimated the reflectivity by 1dB, while the M3 mode overestimated the reflectivity by 2dB. The radial velocities obtained by the three modes were consistent when the velocities were not aliased. L_{DR} biases between the three modes were small when L_{DR} was greater than −25 dBZ. However, when the cross-polar reflectivity was relatively weak, the different benefits from the coherent integration for the three modes introduced large L_{DR} bias.

(3) The M2 mode was found to be able to effectively improve the capability of radar detection by increasing the pulse width. Compared with the M3 mode, the M2 mode improved the capability of measurements by 60% for clouds above 3 km, and by 80% for clouds above 6 km.

(4) Due to the effects of radial velocity aliasing in the M1 mode, only 50% of the M1 reflectivity data below the bright band were used for cloud and precipitation observations. Above this height, more M1 data were used for clouds with moderate reflectivity. Most M2 data were used to observe weaker clouds within the valid detection range of the M2 mode. The merging algorithm reproduced reasonable cloud structures.

Meanwhile, we found that the L_{DR} and velocity spectrum width from the three modes were significantly influenced by the SNR, pulse width, and benefits of coherent integration. Valid measurements of L_{DR} are still limited. The radial velocity resolution from the M1 mode is high, but severe velocity aliasing exists in precipitation measurement. Further optimization of the operational modes and radar calibration are needed to solve these problems.

Acknowledgements. We appreciate the contributions made by the Tibet Meteorology Administration, Naqu Meteorology Administration, and the 23rd Research Institute of China Aerospace & Industry Corp. This study was funded by the National Sciences Foundation of China (Grant No. 91337103) and the China Meteorological Administration Special Public Welfare Research Fund (Grant No. GYHY201406001).

REFERENCES

Clothiaux, E. E., and Coauthors, 1999: The atmospheric radiation measurement program cloud radars: operational modes. *J. Atmos. Oceanic Technol.*, **16**, 819–827.

Clothiaux, E. E., T. P. Ackerman, G. G. Mace, K. P. Moran, R. T. Marchand, M. A. Miller, and B. E. Martner, 2000: Objective determination of cloud heights and radar reflectivities using a combination of active remote sensors at the ARM CART sites. *J. Appl. Meteor.*, **39**, 645–665.

Kollias, P., M. A. Miller, E. P. Luke, K. L. Johnson, E. E. Clothiaus, K. P. Moran, K. B. Widener, and B. A. Albrecht, 2007: The atmospheric radiation measurement program cloud profiling radars: second-generation sampling strategies, processing, and cloud data products. *J. Atmos. Oceanic Technol.*, **24**, 1119–1214.

Liu, L. P., L. Xie, and Z. H. Cui, 2014: Examination and application of Doppler spectral density data in drop size distribution retrieval in weak precipitation by cloud radar. *Chinese Journal of Atmospheric Sciences*, **38**(2), 223–236. (in Chinese with English abstract)

Liu, L. P., J. F. Zheng, Z. Ruan, Z. H. Cui, Z. Q. Hu, S. H. Wu, G. Y. Dai, and Y. H. Wu, 2015: Comprehensive radar observations of clouds and precipitation over the Tibetan plateau and preliminary analysis of cloud properties. *Journal of Meteorological Research*, **29**, 546–561.

Moran, K. P., B. E. Martner, M. J. Post, R. A. Kropfli, D. C. Welsh, and K. B. Widener, 1998: An unattended cloud-profiling radar for use in climate research. *Bull. Amer. Meteor. Soc.*, **79**, 443–455.

Zhong, L. Z., L. P. Liu, S. Feng, R. S. Ge, and Z. Zhang, 2011: A 35-GHz polarimetrie Doppler radar and its application for observing clouds associated with typhoon Nuri. *Adv. Atmos. Sci.*, **28**(4), 945–956, doi: 10.1007/s00376-010-0073-5.